NASA

Technical Memorandum 79656

The MAGSAT Vector Magnetometer — A Precision Fluxgate Magnetometer for the Measurement of the Geomagnetic Field

M. H. Acuna, C. S. Scearce,
J. B. Seek and J. Scheifele

RECEIVED
NASA STI FACILITY
ACCESS DEPT.

October 1978

THE MAGSAT VECTOR MAGNETOMETER - A PRECISION FLUXGATE

MAGNETOMETER FOR THE MEASUREMENT OF THE GEOMAGNETIC FIELD

by

M.H. Acuna, C.S. Scearce, J.B. Seek, J. Scheifele
Planetary Magnetospheres Branch
Laboratory for Extraterrestrial Physics
NASA/Goddard Space Flight Center
Greenbelt, Maryland 20771

ABSTRACT

A description of the precision triaxial fluxgate magnetometer to be flown aboard the MAGSAT spacecraft is presented. The instrument covers the range of $\pm$ 64,000 nT with a resolution of $\pm$ 0.5 nT, an intrinsic accuracy of $\pm$ 0.001% of full scale and an angular alignment stability of the order of 2 seconds of arc. It was developed at NASA's Goddard Space Flight Center and represents the state-of-the-art in precision vector magnetometers developed for spaceflight use.

INTRODUCTION

The general objectives of the MAGSAT mission are the acquisition of accurate magnetic field data from a low polar orbiting spacecraft to obtain an accurate and up-to-date quantitative description of the geomagnetic field as well as the compilation of global scalar and vector crustal magnetic anomaly maps. The instrumentation aboard the MAGSAT spacecraft consists of an alkali vapor scalar magnetometer, a precision vector magnetometer and an attitude determination system composed of two star cameras, a precision sun sensor and a boom attitude transfer system. A more detailed description of the mission and its objectives has been given by Langel[1].

The accuracy goals for the mission require a vector magnetometer capable of measuring the geomagnetic field with a maximum error of $\pm$ 1 nT in magnitude and 5 seconds of arc in direction. The development of such an instrument within the constraints imposed by the spacecraft and its subsystems represents a major technological achievement which would not have been possible without parallel developments in the areas of ultraprecision linear integrated circuits and passive components. The design presented here

2

represents a compromise among many conflicting requirements and limitations
imposed by reliability considerations, available resources and state-of-the-
art components. Other implementaticn schemes are undoubtedly possible with
equivalent performance but their incompatibility with the spacecraft and
other instruments precluded their utilization.

INSTRUMENTATION

A block diagram of the Vector Magnetometer is shown in Figure 1.
The instrument consists of a basic triaxial fluxgate magnetometer with a
dynamic range of $\pm$ 2000 nT, a 12-bit analog-to-digital converter and
three 7-bit digital-to-analog converters which are used as field offset
generators for each orthogonal axis to increase the measurement dynamic
range to $\pm$ 64,000 nT in steps of $\pm$ 1000 nT. The bias steps are automatically
added or subtracted depending on the magnitude of the external field, to
maintain the fluxgate magnetometer within its operating range, as shown in
Figure 2.

This approach yields $\pm$ 0.5 nT resolution and is equivalent to utilizing
a magnetometer with a $\pm$ 64,000 nT dynamic range in conjunction with a
17-bit analog-to-digital converter. The reasons for choosing this
"differential measurement" approach are basically considerations of
dynamic response of a 17-bit A/D converter, magnetometer feedback loop
stability and slew rate, as well as zero level offset stability versus
a.c. gain. Some of these tradeoffs are presented below where the magnetometer
electronics and transfer function are discussed. The external magnetic
field is not expected to change appreciably between samples and the
differential approach with a basic "window width" of $\pm$ 1000 nT is more
than adequate.

The magnetic field is sampled 16 times per second along each of the three orthogonal directions and the field offset generator is updated at the same rate. Thus, if we assume that a 64,000 nT field is suddenly applied to the sensor, it takes approximately 4 seconds (64 x .0625) for the field offset generator to step to the proper level and thus obtain a valid measurement. However, this is a worst case situation since we are dealing with a non-spinning spacecraft and the external field does not vary significantly between samples.

The digital data corresponding to the 'fine' (12 bits) and 'coarse' (7-bits) readouts are fed directly to the spacecraft through a serial interface. No on-board processing of data is utilized.

As can be seen from Figure 1, the magnetometer electronics, A/D converter, field offset generators, digital interface and power converter are implemented in a redundant configuration which can be selected by ground command in case of failures. This block redundancy approach provides a fundamental measure of reliability and eliminates from consideration single point failures in the electronics.

The digital interface logic, 12-bit A/D converter and power converter are implemented with conventional designs using CMOS microcircuits and switching regulators respectively, and will not be covered here.

The fluxgate sensor assembly and associated electronics and the field offset generator design are presented below. The last section covers the calibration and alignment procedures utilized to verify instrument performance.

4

TRIAXIAL FLUXGATE SENSOR

The fluxgate sensors are constructed utilizing the ring core geometry which has been shown to exhibit superior performance characteristics in terms of drive power requirements, long term zero stability and noise level when compared to other types of fluxgate sensors. The magnetic material used in these sensors is an advanced molybdenum permalloy especially developed for the GSFC-Voyager Magnetic Field Experiment in cooperation with the Naval Surface Weapons Center, White Oak, Maryland. It exhibits extremely low noise and high stability characteristics typical of 6-81 Mo.Pe. alloys developed for fluxgate magnetometer applications by the NSWC group. The use of these alloys and the ring core sensor geometry allows the realization of compact, ultrastable fluxgate sensors with unmatched performance.

A schematic drawing showing the construction of each sensor is shown in Figure 3 while the triaxial sensor assembly is shown in Figure 4. Crucial elements in the design of the MAGSAT sensor are the feedback coil which nulls the ambient field and the sensor core itself since they can be shown to be the most significant sources of error, both from alignment stability point of view as well as the scale factor stability versus temperature.

The approach utilized here is to use individual axis nulling, that is, each axis is nulled independently in only one direction. This is the most common approach but suffers from extreme sensitivity to cross-fields since the ambient field is nulled only along the sensor axis. Thus any distortion or motion of the sensor core within the feedback coil represents an effective alignment change due to the presence of the transverse field.

5

An approach that minimizes this sensitivity is to use a relatively
large triaxial Helmholtz coil system around the triaxial sensor such that
the external field is nulled over the entire sensor volume rather than just
along each axis individually. However, the large dimensions of the coil
system introduce additional complications in terms of alignment stability,
thermal control and particularly in the case of the MAGSAT spacecraft,
the generation of relatively large fields at the location of the scalar
magnetometer due to the feedback current. Hence, the individual axis
nulling approach was selected for implementation.

A rigid attachment of the sensor core to the feedback coil usually
results in differential expansion stresses being transmitted to the
sensor core which can produce significant alignment shifts, zero level
changes as well as dramatic increases in sensor noise levels. These
problems can be solved by carefully matching the thermal expansion
coefficients of the elements involved (core, windings, support structure)
to minimize differential stresses and changes in the relative geometry
between the core and the feedback coil.

In Figure 5 we show the relative variation of the feedback field
versus relative dimensional changes, both isotropic and anisotropic,
introduced by temperature variations for a coil having a geometry similar
to that utilized in the MAGSAT sensors, and a variety of structural
materials. The computed field is that at the geometrical center of the
coil but it can be easily shown that the field intensity at any point
within the coil follows a similar variation as a function of temperature.
From the figure and formulas it can be seen that the dominating factor
is the variation of coil length with temperature. Since the sensor
responds to a weighted average of the magnetic field over an undetermined
volume in space, the proceeding calculation constitutes a zeroth-order
approximation to the actual behavior of the sensor. Nevertheless,
the general temperature dependence shown in Figure 5 was verified
for prototype instruments utilizing a 50,000 nT field "trapped"
in a 15 cm superconducting shield and varying the sensor temperature
over -40°C to $+60^{\circ}$C.

The fundamental strategy followed for MAGSAT was to match the expansion coefficient of the support structure and windings to that of the sensor core itself ($\sim 11 \times 10^{-6}/^{o}C$). Of the structural materials shown in Figure 5, MACOR* was selected due to its expansion coefficient (10×10^{-6}) zero water absorption (and thus dimensional stability versus relative humidity changes) and ease of machinability. The feedback coil was wound with polyurethane-nylon insulated platinum wire with a linear thermal expansion coefficient of $9.9 \times 10^{-6}/^{o}C$.

In terms of alignment stability the small dimensions of the sensor require structural deformations to be smaller than 51 microns under all environmental conditions to obtain the desired alignment stability of 5 arc seconds. This extreme requirement necessitated the use of extremely stable, hysteresis free materials for the feedback coil and support structure, such as MACOR*, while the mounting surfaces were polished flat to a surface roughness of < 10 μ prior to assembly. By closely matching the expansion coefficients of the sensor and feedback coil it was possible to rigidly bond these two components together and thus minimize relative displacements. The only remaining source of error is motion of the actual magnetic material within the core bobbin. This constituted a significant problem in spite of the close tolerances used during sensor core manufacture. The solution found was to increase the amount of magnesium oxide normally used to insulate the tape material, such as to fill the entire support bobbin and completely enclose the tape. This solution proved very effective in vibration and environmental tests performed on a prototype sensor and no alignment shifts were detected.

* Corning Glass Works trademark

Since the overall expansion coefficient of the feedback coil is non-zero the magnitude of the feedback field, that is, the scale factor, will be a function of temperature as shown in Figure 5. In the magnetometer electronics description given below, we show how this temperature dependence can be compensated for over a wide temperature range by means of a modified current source designed to produce a constant feedback field as a function of temperature.

The external magnetic field generated by this sensor arrangement is less than $\pm$ 1 nT at 46 cm from the sensor when measuring fields of $\pm$ 64,000 nT. This low field value minimizes the interference with the alkali vapor scalar magnetometer which is located only 43 cm away from the sensor assembly.

As shown in Figure 4, two MACOR* optical cubes are bonded to the sensor mount to obtain accurate angular position determination during alignment tests described in the last section of this paper. The sensor assembly is mounted on a temperature stabilized baseplate which also supports two large mirrors associated with the Attitude Transfer System (ATS). Temperature stabilization of this baseplate is required to minimize optical alignment shifts between the sensor optical cubes and the ATS mirrors due to the different thermal expansion coefficients involved.

MAGNETOMETER ELECTRONICS

The electronics design of the MAGSAT Vector magnetometer incorporates a number of developments derived from the Voyager Magnetic Field Experiment (Acuna,[2]; Behannon et al.,[3])which are directly applicable to the present instrument. Figure 6 shows a block diagram of the basic

8

fluxgate magnetometer while a detailed schematic of the drive and signal

processing electronics for each axis is shown in Figure 7. A 250 kHz

synchronization signal is derived from the spacecraft clock and divided

down to 12.5 KHz to provide the excitation signal for the fluxgate sensors.

A high efficiency 'capacitive discharge' circuit is utilized to drive

the cores to over 100 times their coercive force with low average power

requirements (Acuna[2]). The peak-to-peak sensor drive current is

approximately 600 mA while the average drive power requirement is only 70 mW.

This arrangement essentially eliminates the problem of 'perming' of flux-

gate sensors for externally applied fields of up to 20 gauss. The simple

voltage regulator used in the driver stage ensures the stability of the

drive signal amplitude over all environmental conditions.

The signal processing electronics consist of an A.C. preamplifier

tuned to the second harmonic of the drive signal, a synchronous

demodulator, an operational integrator and a transconductance feedback

summing amplifier which takes the place of the feedback resistor in

conventional designs. A low pass, 6 db/octave filter is utilized at

the output to limit the signal bandwidth to 8 Hz since as mentioned

previously, the sampling rate is 16 samples/sec.

The input circuit to the A.C. preamplifier incorporates a tuned

secondary transformer while the primary side presents a low impedance

to the fluxgate sensor. The inductance of the sense/feedback sensor

winding is series tuned with the input capacitor and reactive part of

the input impedance to obtain considerable amplification of the second

harmonic signal in the sensor itself through negative resistance

parametric amplification (Acuna[2]). The amount of parametric

amplification obtained in the MAGSAT sensors is considerably smaller than in other similar fluxgate sensors due to the high resistance of the feedback winding which is constructed using insulated platinum wire. Nevertheless, the overall sensitivity achieved of 100 μV/nT at the secondary of the input transformer (compared to 10 mV/nT for copper wound coils) is more than adequate to obviate the need for an ultra-high gain A.C. preamplifier and its associated problems. A simple two-stage, hybrid preamplifier with a low noise FET at the input provides a gain of approximately 75. A low Q tuned circuit is included at the output to provide additional rejection to unwanted odd frequency components which could affect the performance of the non-ideal synchronous detector.

The low input impedance of the preamplifier essentially eliminates the problem of sensor cable length affecting the tuning of the input stage and allows a significant increase in the (2nd harmonic/fundamental) ratio applied to the first active device. All these features combine to produce an instrument remarkably free of 'electronic perm' and extremely temperature stable.

The synchronous detector is a conventional design utilizing a quad CMOS transmission gate driven by a second harmonic reference signal derived from the frequency divider chain in the drive electronics. The operational integrator provides the bulk of the gain in the loop and its time constant is selected to guarantee loop stability and the desired response bandwidth. The transfer function of the instrument is discussed in more detail below.

10

The output of the integrator is applied to the trasconductance amplifier and the output low pass filter. The amplifier is configured as a modified voltage controlled current source which sums in the proper ratio (32:1) the signals from the integrator and the field offset generator. This is the most crucial element in the design since it determines the accuracy and stability of the magnetometer scale factor. In the previous section we discussed the problem of scale factor dependence upon temperature due to thermal expansion of the feedback coil. In order to compensate for this effect we have taken advantage of the significant variation of feedback coil resistance with sensor temperature to maintain the feedback field constant.

Since the variation of this field is, to a first approximation, mainly dependent upon coil length variations (see Figure 5), we can write

$$\vec{B}_f = \frac{K \, I_f}{\ell(1 + \alpha_M T)} \tag{1}$$

where I_f is the feedback coil current, K a proportionality constant, ℓ the coil length, α_M the thermal expansion coefficient of the support bobbin and coil wire (matched), and T the ambient temperature. In addition the feedback coil resistance varies with temperature as

$$R_c = R_o (1 + \alpha_p T) \tag{2}$$

where R_o is the reference temperature resistance value and α_p the thermal resistivity coefficient for the coil wire.

Considering now the simplified schematic for the feedback amplifier shown in Figure 8, the current through the coil is given by

11

$$I_f = \frac{-(E_1 + E_2)}{R_1 + R_0(1+\alpha_p T)\left[\dfrac{R_1+R_2-R}{(R/2) + R_2}\right]}$$ (3)

Introducing this equation in (1), differentiating with respect to T and ignoring second order terms of $O(\alpha_M \alpha_p)$, we find that if we choose

$$R_2 = \frac{\beta(R-R_1) - (R/2)}{1 + \beta}$$ (4)

where

$$\beta = \frac{R_0}{R_1}\left(1 + \frac{\alpha_p}{\alpha_M}\right)$$ (5)

then the feedback field, as defined by Equation (1) will be independent of temperature. Basically, the circuit incorporates a slight amount of positive feedback to compensate for the decrease of $\vec{B}_f$ due to coil expansion. It is then possible to adjust R_2 such as to make the scale factor dependence with temperature as small as possible.

This compensation approach has been used with excellent results in several fluxgate variometers built at GSFC for ground based studies of the geomagnetic field.

The operational amplifier used in this circuit is an ultrastable (0.1 $\mu V/^oC$ ΔVos) monolithic unit with excellent long term stability characteristics and very low noise. Other amplifier types were considered such as monolithic choppers, but were not used due to either noise performance, reliability or long term stability considerations.

The resistors associated with this circuit are ultraprecision, hermetically sealed units with an absolute temperature coefficient of < 0.5 ppm/$^{\circ}$C. Tracking characteristics approach 0.2 ppm/$^{\circ}$C, while long term stability after initial conditioning is of the order of 20 ppm/yr.

Since the maximum allowable error voltage at the amplifier input is only 125 μV (1 nT), considerable attention was given to thermally generated e.m.f.'s which can be produced across dissimilar metal junctions. The circuit layout is such that thermal gradients across critical paths are minimized by close proximity of conductors. Low thermal solder was used during assembly to further reduce the magnitude of the e.m.f.'s generated across solder joints.

The detailed circuits shown in Figure 7 also incorporate means for reversing upon command the phase of the sensor and second harmonic reference signals. This allows the detection of unexpected electronic offsets which could develop during operation in orbit.

MAGNETOMETER TRANSFER FUNCTIONS

Since the post-detection bandwidth of the system is much smaller than the passband associated with the preamplifier tunded circuits, the closed loop transfer function for the magnetometer (not including the output low-pass filter) can be well approximated by

$$H(S) = \frac{1}{S^2 \left(\dfrac{\tau_1 \tau_2}{K_1 A_p G_m} \right) + S \left(\dfrac{\tau_2 + \tau_3}{K_1 A_p G_m} \right) + 1} \tag{6}$$

where τ_1, is the synchronous defector time constant, τ_2 the integrator time constant, A_p is the preamplifier gain and K_1 the sensor sensitivity in [Volts/Amp]; G_m is the equivalent transconductance of the feedback amplifier. In the MAGSAT design, the output filter for the synchronous detector is not isolated from the integrator and this causes a small time constant $\tau_3 \ll \tau_2$ to be added to the integrator time constant in the second term of the denominator of (6). In analogy to a second order system,

we can define

$$\omega_n^2 = \frac{K_1 A_p G_m}{\tau_1 \tau_2} \qquad (7)$$

$$\frac{2\zeta}{\omega_n} = \frac{\tau_2 + \tau_3}{K_1 A_p G_m} \qquad (8)$$

Hence, given ζ and ω_n we can select the time constants τ_1 and τ_2 to satisfy equations (7) and (8). For this instrument the closed loop 3 db cutoff frequency was selected as 50 Hz and $\zeta = 0.7$. The output filter reduces the bandwidth to 8 Hz and its response for frequencies near and above the cutoff is then closely approximated by a 6 db/oct rolloff first order low-pass filter.

The values computed from equations (7) and (8) ensure loop stability and the desired small signal frequency response. However, for large output amplitudes, the response may be limited by the maximum obtainable slew rate at the output of the integrator,

$$SR_{max} = \frac{E_{omax} \text{ (synchronous detector)}}{\tau_2} \qquad (9)$$

Here E_{omax} is the maximum output voltage ($\sim \pm 6$ volts) which can be obtained from the synchronous detector. From equations (7) and (8) we can observe that large values of $K_1 A_p$ (sensor-preamplifier gain) require large values of τ_2 (integrator time constant) for stability. This leads to reduced values of maximum slew rate, limiting the amplitude of high frequency signals that can be followed by the instrument. On the other hand, small values of $K_1 A_p$ lead to significant and temperature dependent zero level errors due to variations in the

14

synchronous detector and integrator "effective" offset errors with temperature. Thus the choice of ω_n, ζ and $K_1 A_p$ has to be carefully analyzed for loop stability and obtainable slew rate. Large values of ω_n accompanied by large values of ζ (overdamped system), selected to obtain the desired 3 db rolloff frequency, lead to larger values of maximum slew rate.

In the present design, the maximum slew rate is $\sim$ 9000 volts/sec. which, if we consider the maximum output amplitude of 8 volts, corresponds to an output frequency of 180 Hz, well beyond the loop cutoff.

The above considerations were taken into account in selecting the present implementation approach for the instrument. A magnetometer with a dynamic range of $\pm$ 64,000 nT and equivalent zero level stability performance would have required an integrator time constant 32 times larger than the present design. Note that in either case the same slew rate in terms of field amplitude, 2.25×10^6 nT/sec, is obtained.

FIELD OFFSET GENERATOR

A simplified diagram of the field offset generator is shown in Figure 9. This is a conventional design utilizing an R-2R resistor ladder network. Low "ON" resistance junction field effect transistors with ultra-low leakage currents are utilized for the switches, while the operational amplifier is the same as that used in the magnetometer feedback loop. The ladder is used in the current mode to minimize common mode errors associated with the amplifier.

The same considerations regarding thermal e.m.f.'s discussed for the feedback amplifier apply to this circuit. The ladder resistors are ultraprecision custom units matched to a tolerance of $\pm$ 0.001% to simplify the calibration and data reconstruction procedures.

15

The voltage reference was implemented around a temperature stabilized precision zener (LM199A) which was subjected to a 1000 hour screening test for long term stability.

The digital inputs to the offset generator switches are derived from an up-down counter associated with the 12-bit A/D converter logic. When the 'fine' digitized signal for a given axis exceeds an upper or lower threshold ($\pm$ 1000 nT), the counter is allowed to count up or down respectively, to maintain the magnetometer within its operating range.

CALIBRATION AND ALIGNMENT

The problem of determining the orientation of a magnetic field vector has traditionally been solved by assuming that the field orientation can be accurately established by the geometry of a calibration coil system. This method is generally sufficient to determine sensor orientations within a few minutes of arc from its true direction but it is certainly not adequate for the present case where accuracies of the order of 2 seconds of arc are required. The method utilized to determine the sensor alignment was similar in principle to that presented by McPherron and Snare[4] except that only two sensor rotations are required and the system of equations to be solved is considerably simplified. A detailed description of the modified method has been given by Acuna[5].

The basic assumption made is that if the deviations from orthogonality of the sensor assembly and triaxial test coil system are small (within a few degrees), the measurements obtained from a sensor mounted perpendicular to the field direction will reflect the sum of the deviations of the sensor and test coil systems.

16

An optical reference coordinate system is first accurately established
by means of a pair of first order theodolites which are rigidly mounted
to suitable supports, leveled and referenced to a stable azimuth direction.
This azimuth reference was established by means of two anchored concrete
piers, separated by approximately 400 meters, outside the magnetics test
facility.

The magnetic field vectors in the reference and coil coordinate
systems are related by a transformation matrix

$$\vec{H}_{ref} = [B] \vec{H}_{coil} \tag{10}$$

and the measurements in the sensor coordinate system are related to the
reference coordinate system

$$\vec{M}_{sensor} = K [A] \vec{H}_{ref} \tag{11}$$

where $\vec{M}_{sensor}$ represents the measured vector when a vector $\vec{H}_{ref}$ is applied
in the reference system, and K is the scale factor proportionality constant.

Thus, when the sensor is tested in the coil system, its output
can be written as

$$\vec{M}_{sensor} = K[A] [B] \vec{H}_{coil} \tag{12}$$

and under the assumption that [A] and [B] are nearly diagonal

$$\vec{M}_{sensor} \cong K \{ [I] + [\delta A] + \delta[B] \} \vec{H}_{coil} \tag{13}$$

where $[\delta A]$ and $[\delta B]$ are the orthogonality deviation matrices.
In order to determine all the off-diagonal elements of [A] and [B] it is
necessary to obtain measurements for three sensor positions differing

from the previous one by an exact 90° rotation established by the
optical system, and by energizing each test coil system axis independently.
The procedure thus yields not only the sensor alignment with respect to
the reference coordinate system, but also the matrix [B], the test coil
system alignment simultaneously.

The advantages of this method are numerous, but the most important
is that the test coil system is only required to be structurally stable
for the duration of one alignment test ($\sim$ 1 hour). The ultimate accuracy
obtainable with this method is determined by the stability and noise
characteristics of the magnetic test facility. In the case of the
GSFC 6.7 meter Helmholtz coil system, the 'equivalent noise' is approxi-
mately 1.5 seconds of arc.

The magnetometer scale factor is calibrated using a proton precesion
magnetometer for fields above 20,000 nT. For small fields, the calibra-
tion constants are synthesized from selected incremental measurements
above 20,000 nT such as to determine the exact 'weights' of each of the
7 bits in the offset generator.

SUMMARY

A description of the MAGSAT Precision Vector Magnetometer has been
presented. The instrument represents the state-of-the-art in precision
vector magnetometers and covers the range of $\pm$ 64,000 nT using a
$\pm$ 2000 nT basic magnetometer and field offset generators. The design
utilizes ultraprecision components and electronic compensation of the
scale factor temperature dependence by sensing the changes in resistance of the
feedback coil. Brief discussions of the instrument transfer function, dynamic
response and sensor alignment determination method were presented. A
summary of the instrument performance characteristics is given in Table 1.

ACKNOWLEDGMENTS

REFERENCES

[1] R. A. Langel, R. D. Reagan, J. P. Murphy, MAGSAT: A Satellite for
     Measuring near Earth Magnetic Fields, GSFC X-922-77-199, July 1977.

[2] M. H. Acuna, Fluxgate Magnetometers for Outer Planets Exploration,
     IEEE Trans. Magnetics, Vol. MAG-10, 3, 519, September 1974.

[3] K. W. Behannon, M. H. Acuna, L.F. Burlaga, R. P. Lepping, N. F. Ness,
     and F. M. Neubauer, Magnetic Field Experiment for Voyagers 1 and 2,
     Space Science Reviews, 21, 235-257, 1977.

[4] R. L. McPherron and R. C. Snare, A Procedure for Accurate Calibration
     of the Orientation of the Three Sensors in a Vector Magnetometer,
     IEEE Trans. Geoscience Electronics, Vol. GE-16, 2, 134-137, April 1978.

[5] M. H. Acuna, MAGSAT-Vector Magnetometer Absolute Sensor Alignment
     Determination, NASA-GSFC Technical Memorandum 79648, September 1978.

TABLE 1

MAGSAT – PRECISION VECTOR MAGNETOMETER

SUMMARY OF TECHNICAL CHARACTERISTICS

BASIC FLUXGATE MAGNETOMETER

Dynamic Range: ± 2000 nT

Resolution (12-bit A/D):   ± 0.5 nT

Noise: (8 Hz BW)   0.008 nT RMS

Zero level stability:

    Sensor (-60°C to +60°C)   ± 0.2 nT

    Electronics (-20°C to +50°C)   ± 0.2 nT

Drive Frequency: 12.5 KHz

Linearity error: $< 1 \times 10^{-5}$

OFFSET FIELD GENERATOR: FIELD COMPENSATION UNIT

Dynamic Range: ± 64,000 nT

Quantization Step: 1000 nT

Temperature Coefficient: < 0.5 ppm/°C

Long Term Stability: $< 2 \times 10^{-5}$/year

SENSOR ASSEMBLY

Mass: 0.6 Kg

Dimensions: 11.4 x 5.72 x 5.8 cm

ELECTRONICS (redundant):

Mass: 2.6 Kg

Dimensions: 22.23 x 17.8 x 11.4 cm

Total Power Consumption: @ 25°C   1.8 watts
   @ 0°C   2.0 watts
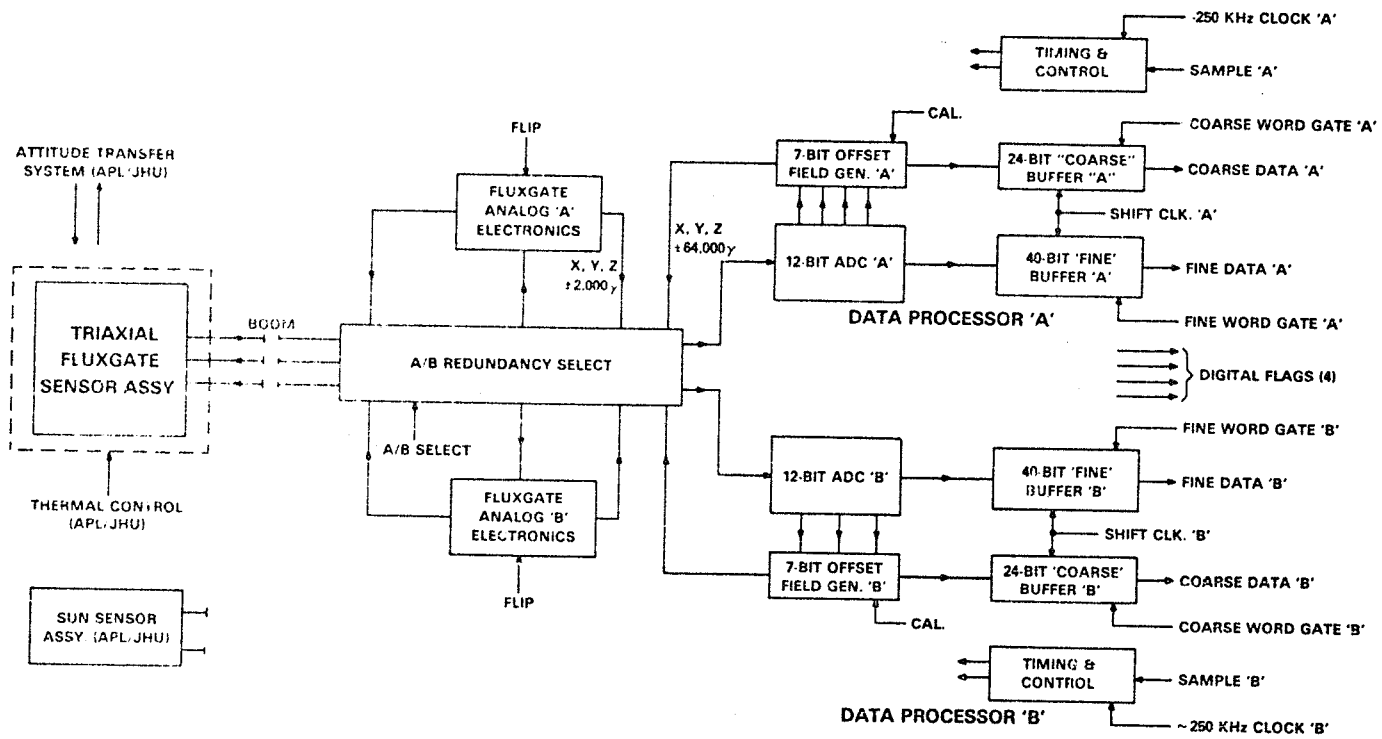
MAGSAT VECTOR MAGNETOMETER
BLOCK DIAGRAM

FIGURE 1
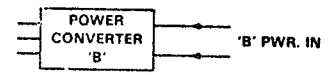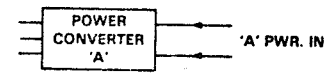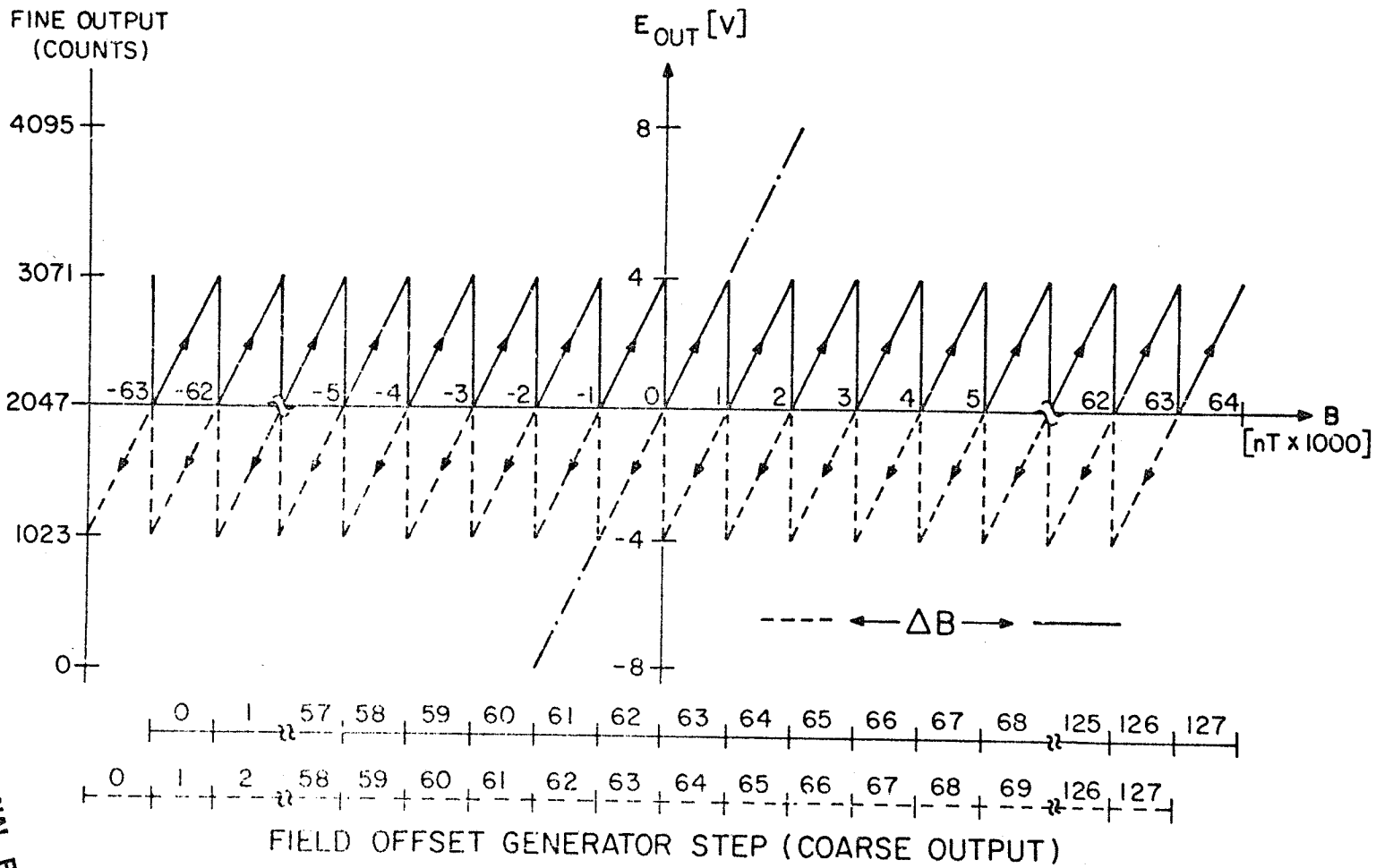
MHA 5-31-77

FIGURE 2

CENTER SUPPORT

DRIVE

FEEDBACK
COIL

CORE

FIGURE 3

MIRROR (.750 CUBE)
(TYP BOTH SIDES)

2.30"

2.25"

4.50"
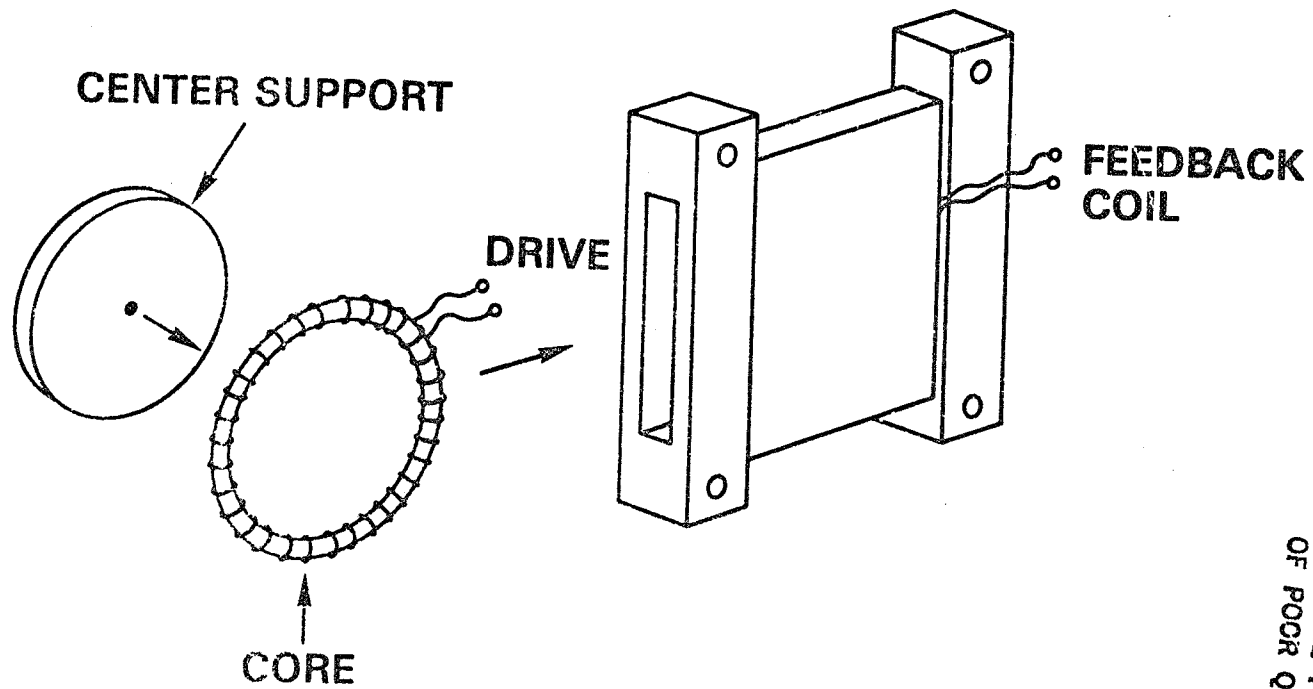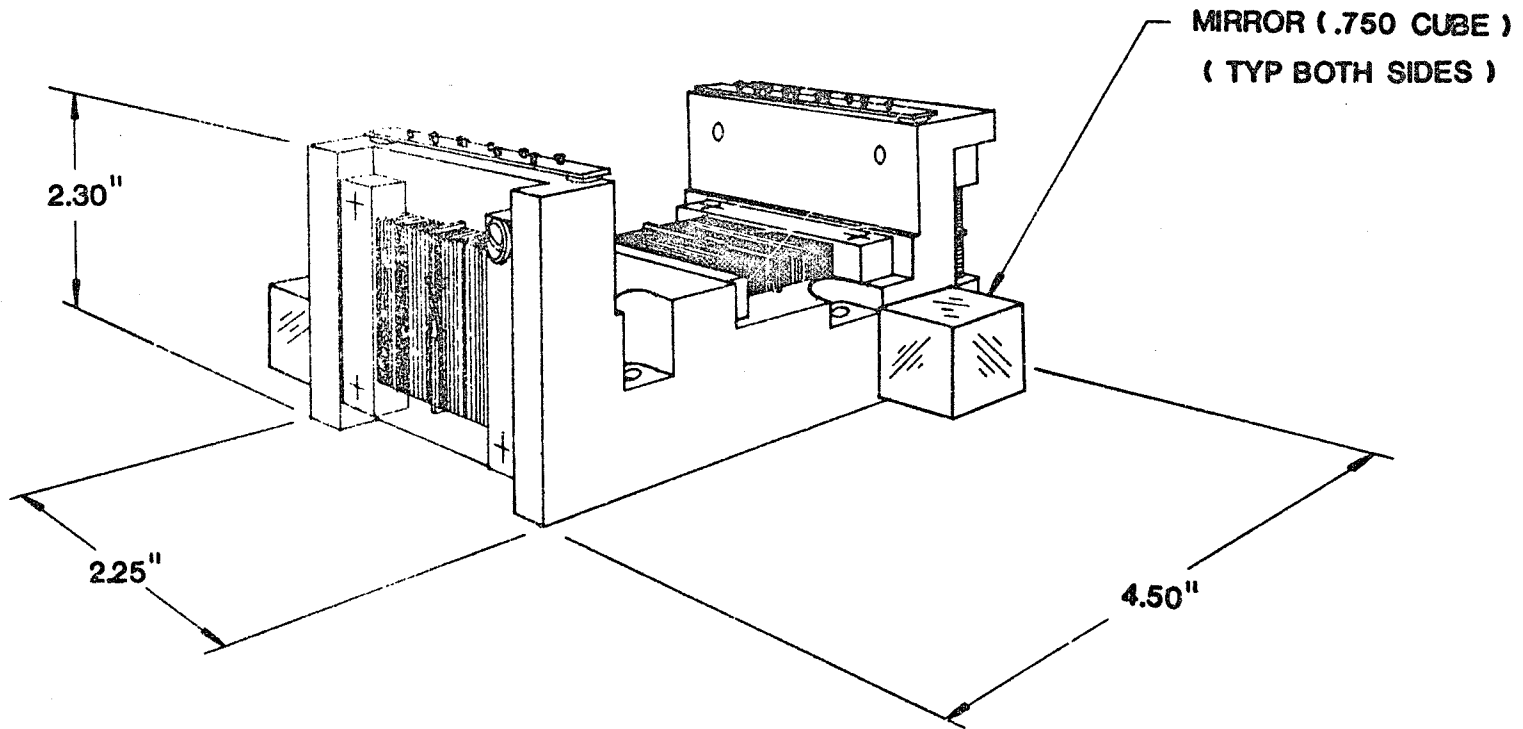
VECTOR MAGNETOMETER SENSOR
MAGSAT

FIGURE 4
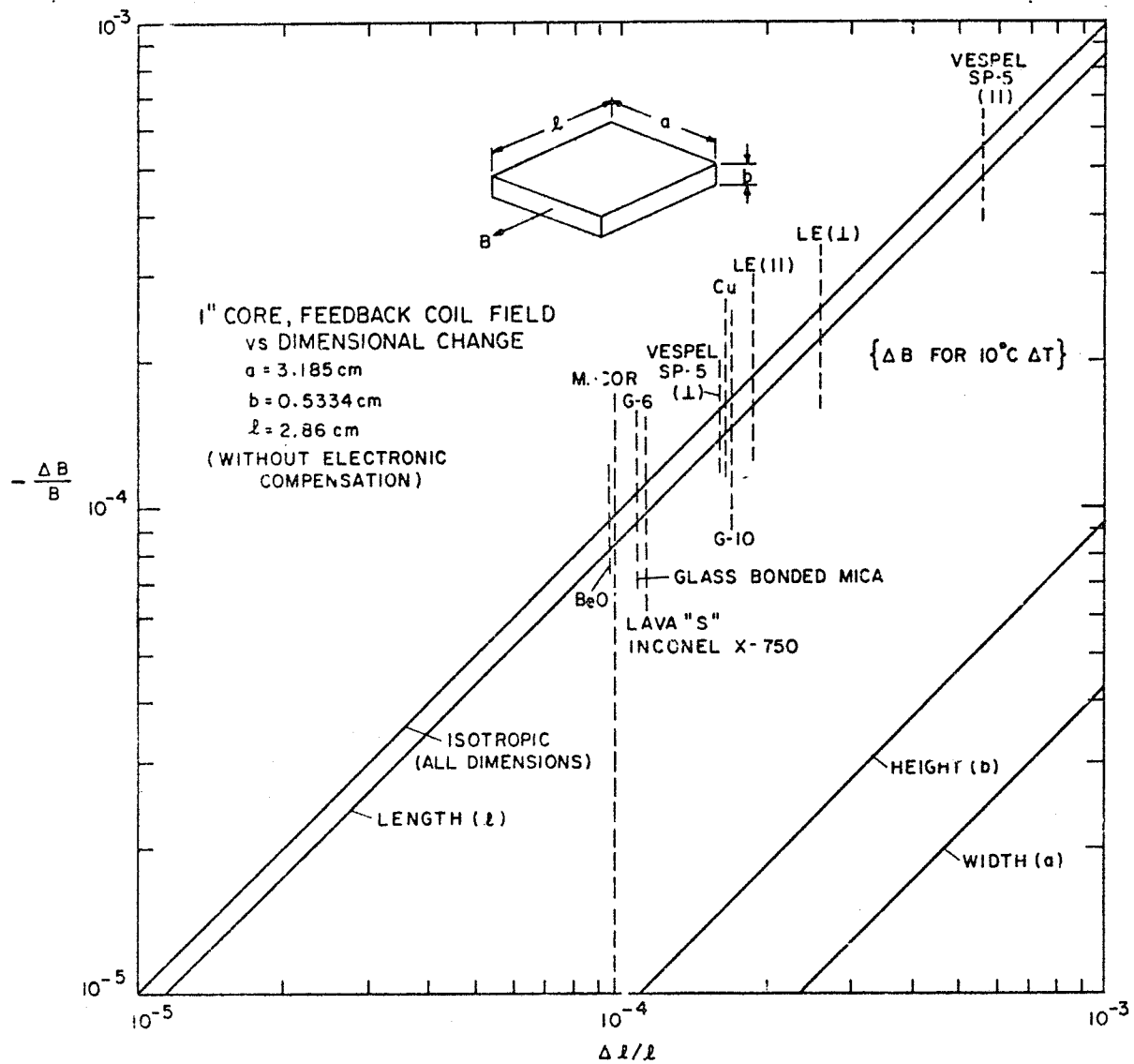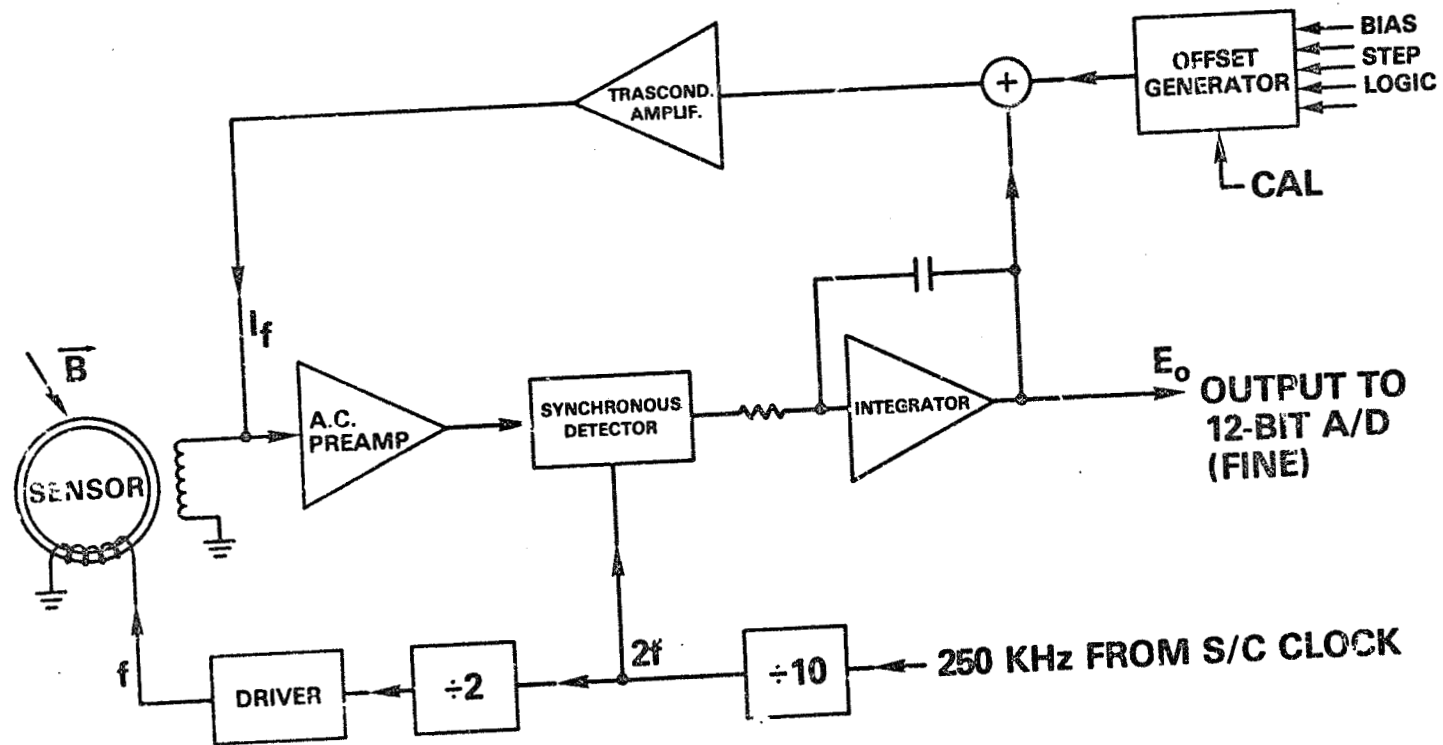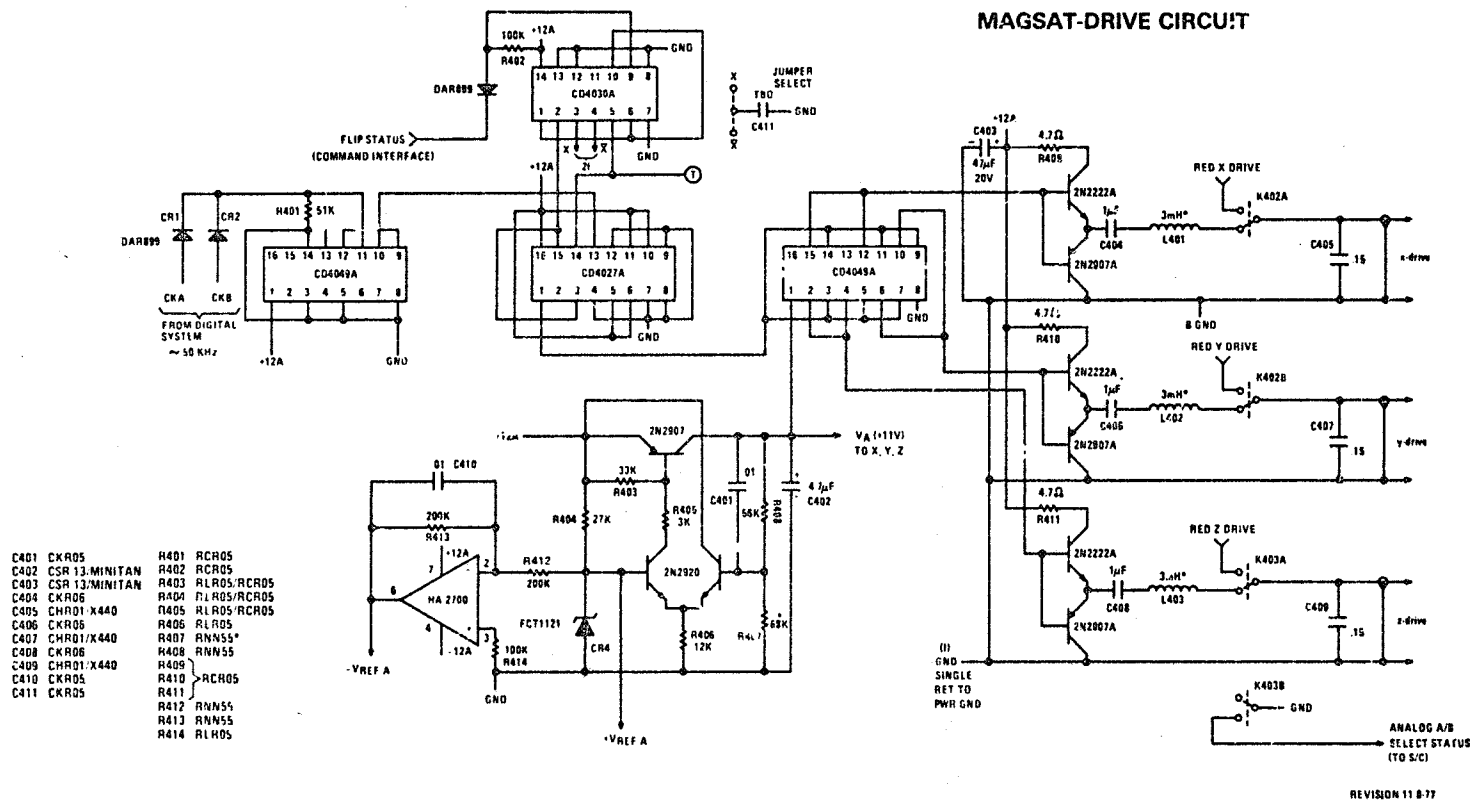
FIGURE 5

FIGURE 6

FIGURE 7(a)

MAGSAT VECTOR MAGNETOMETER
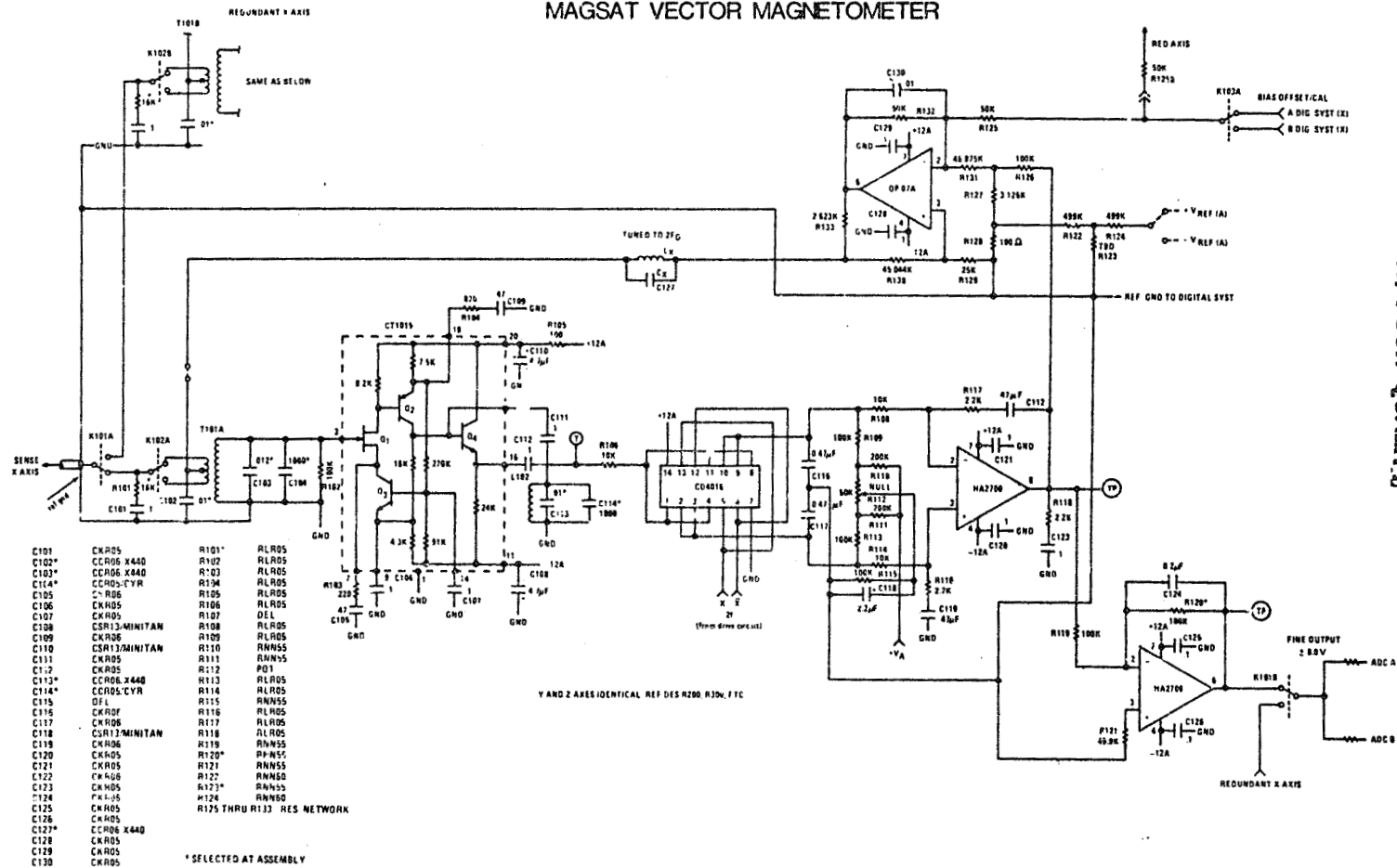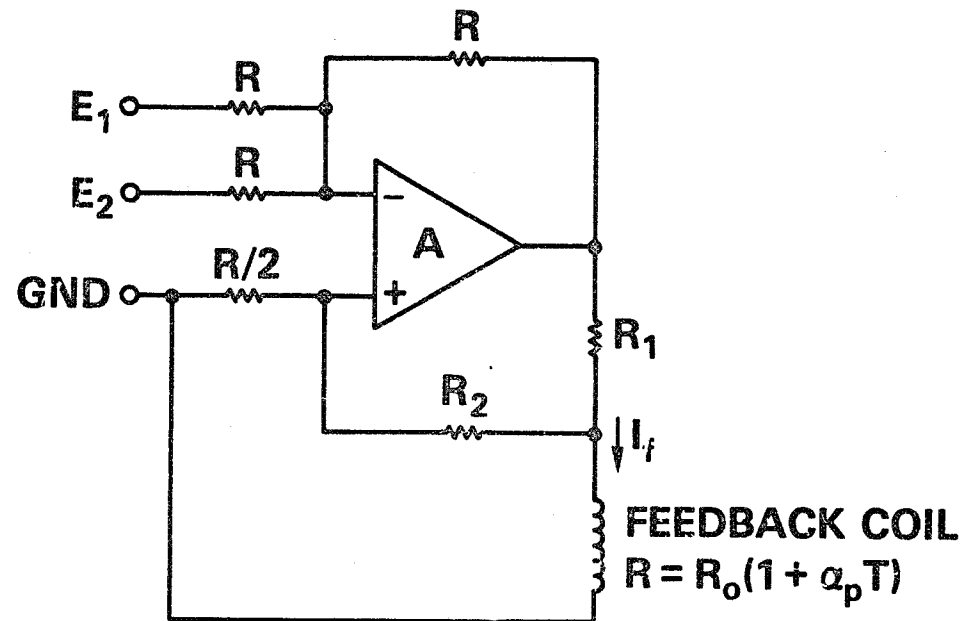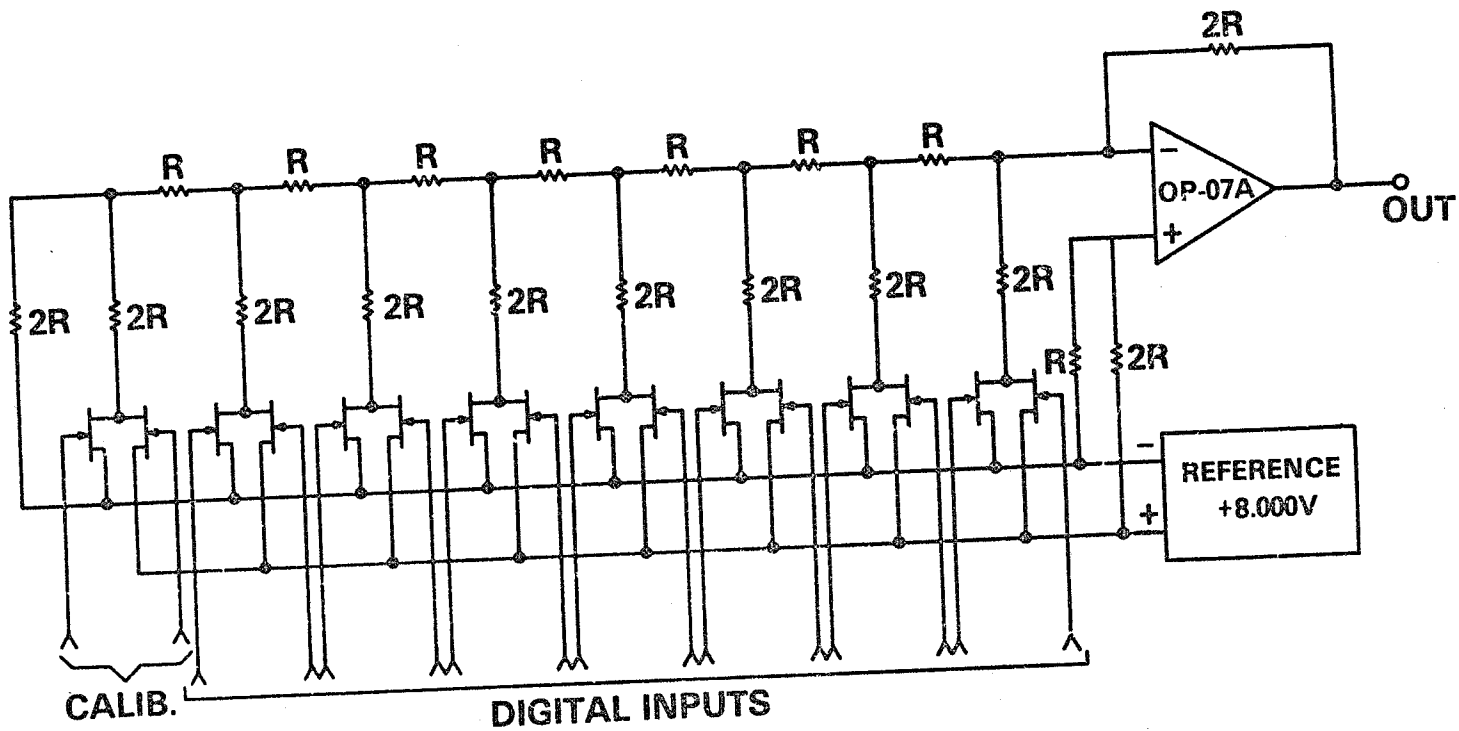
FIGURE 7(b)

FIGURE 8

FIGURE 9

END
DATE
FILMED

APR 26 1979